Applied Catalysis B: Environmental 136–137 (2013) 40–47

Contents lists available at SciVerse ScienceDirect

Applied Catalysis B: Environmental

journal homepage: www.elsevier.com/locate/apcatb

Photocatalytic nitrate reduction in water: Managing the hole scavenger and reaction by-product selectivity

K. Doudrick[a,*], T. Yang[a,b], K. Hristovski[a,c], P. Westerhoff[a]

[a] Arizona State University, School of Sustainable Engineering and The Built Environment, Tempe, AZ 85287-5306, United States
[b] Northwest A&F University, College of Water Resources and Architectural Engineering, Yangling, Shaanxi 712100, PR China
[c] Department of Engineering, College of Technology and Innovation, Arizona State University – Polytechnic Campus, 7171 E. Sonoran Arroyo Mall, Mesa, AZ 85212, United States

ARTICLE INFO

Article history:
Received 14 August 2012
Received in revised form 18 October 2012
Accepted 16 January 2013
Available online 7 February 2013

Keywords:
Titanium dioxide
Photocatalysis
Silver
Nitrate
Formate
Hole scavenger

ABSTRACT

Nitrate contamination of groundwater limits it use as a drinking water supply unless the nitrate is removed. The aim of this study was to move toward implementing photocatalysis for nitrate treatment in drinking water systems by understanding the effects of experimental conditions and the mechanisms involved. Specifically, the photocatalytic reduction of nitrate in water was examined using titanium dioxide (Evonik P90) loaded with silver nanoparticles and formate as a hole scavenger (electron donor). Experimental conditions including pH, nitrate concentration, formate concentration, photocatalyst concentration, and silver loading were varied to demonstrate their effect on the rate of nitrate and formate removal as well as by-product selectivity. For drinking water applications, minimization of residual formate is essential to prevent adverse effects in potable water distribution systems (e.g., carbon source for biofilm growth). The experimental stoichiometric requirement for formate indicated that it acts as a two-hole scavenger, which suggests conduction band electrons, rather than radicals, are responsible for nitrate reduction. Using optimal operating conditions, nitrate and formate were efficiently removed at nearly a 1:1 ratio, showing that the residual hole scavenger concentration can be controlled while maintaining an acceptable rate. Compared to P90 alone, the addition of silver nanoparticles improved the rate of nitrate and formate removal significantly, reduced the overpotential for nitrate reduction, and provided a more positive surface charge. The removal rates decreased with increasing pH, which suggests that the reaction is a proton-coupled electron reaction and that adsorption of the constituents is necessary for effective charge transfer. Under acidic conditions (pH = 2.5), nitrogen gases (~85%) and ammonium (~15%) were the final by-products. Between pH 3.5 and 4, a sudden by-product switch occurred to nitrite, suggesting that, at higher pH, a co-catalyst that is efficient at localizing protons is required to move beyond nitrite.

© 2013 Elsevier B.V. All rights reserved.

1. Introduction

Nitrate is a stable, highly soluble ion that poses a risk to human health and has a large impact on the natural nitrogen cycle. It is a known cause of methemoglobinemia, or "blue baby" syndrome, and could be carcinogenic or an endocrine disruptor [1–3]. The USEPA has set a drinking water maximum contaminant limit (MCL) for nitrate of 10 mg-N/L. A recent survey of 5101 wells in the United States revealed that nitrate levels exceed the standard in approximately 8% of wells (20% agricultural, 3% urban, 4% major aquifers), affecting more than 24.6 million people [4]. This makes nitrate the most ubiquitous contaminant found in drinking water sources [5–8], and these pollution levels continue to rise [9]. Ion exchange traditionally has been used to remove nitrate from drinking water sources, but this process leaves behind a highly concentrated brine solution that still requires treatment. Recent advances in biological and catalyst nitrate treatment technologies are promising [10], but technological disadvantages still remain. Photocatalysis as a reduction process is emerging as a potentially viable water treatment process [11] but requires further mechanistic understanding before optimization for drinking water treatment applications.

Photocatalysts are promising materials for water treatment because of their ability to create photogenerated conduction band electrons (e_{cb}^-) and valence band holes (h_{vb}^+), which enable redox reactions with adsorbed aqueous species (see SI for further discussion of photocatalytic mechanisms). Numerous studies report synthesis of new photocatalysts for nitrate reduction [12–37]. Tantalates have been used to reduce nitrate photocatalytically using water as a hole scavenger, but the removal rate and selectivity toward N_2 was poor [27]. Of the photocatalysts examined,

* Corresponding author. Tel.: +480 727 2911.
E-mail address: kdoudric@asu.edu (K. Doudrick).

0926-3373/$ – see front matter © 2013 Elsevier B.V. All rights reserved.
http://dx.doi.org/10.1016/j.apcatb.2013.01.042

titanium dioxide (TiO_2) is the most efficient at reducing nitrate with a high selectivity toward innocuous by-products (e.g., dinitrogen) [12,13,15,19–25,28,30–37]; silver is the best co-catalyst choice [31,34]. Silver is a strong co-catalyst for reactions involving reduction because it is excellent at trapping e_{cb}^- [38]. For nitrate reduction, TiO_2 requires the addition of an organic compound to fill valence band holes (i.e., electron donor) to either decrease recombination or produce reducing radicals. Formic acid is currently the most efficient hole scavenger for nitrate reduction over TiO_2 [31,34,39]. Although studies have been dedicated to the synthesis of new photocatalytic materials for nitrate reduction, relatively little information is available on the applicability of photocatalytic nitrate reduction to drinking water systems, specifically on their rate and products as a function of pH or under conditions in which residual formic acid can be minimized. Residual formic acid in water distribution systems can serve as a carbon source for undesirable biofilm growth.

The aim of this study was to move toward implementing photocatalysis for nitrate treatment in drinking water systems by understanding the effects of experimental conditions and the mechanisms involved. TiO_2/Ag coupled with formic acid as a hole scavenger was used for this purpose. The objectives of this study were to (1) demonstrate the effect of the physical characteristics of the photocatalyst by varying the photocatalyst surface area and the amount of silver loading, (2) demonstrate the effect of the proton-dependent reaction by varying pH, (3) determine the stoichiometric requirement for formate to control residual formate, and (4) provide mechanistic insights on by-product formation and the role of the hole scavenger. Unlike the vast majority of previous studies that simply report "exposure time in photocatalytic reactor," we report our data with respect to photon fluence to advance the application of photocatalytic reduction systems to engineered practice.

2. Experimental methods

2.1. Chemicals and materials

For this study, a new TiO_2/Ag photocatalyst composite was synthesized using P90 as the TiO_2 source, which is a more active commercial TiO_2 photocatalyst for nitrate reduction than P25 [39]. P90 (Evonik, formerly Degussa, >99.5%) was obtained in powder form. It is synthesized using high-temperature flame hydrolysis of $TiCl_4$ in the presence of oxygen and hydrogen. It contains both anatase (88%, 12 nm) and rutile (12%, 18 nm) crystal structures, has a surface area of approximately 104 m^2/g, and has an average isoelectric point (IEP) of 6.4 [39]. Sodium nitrate ($NaNO_3$, 99%, EMD) was used as the nitrate source and silver nitrate ($AgNO_3$, >99%, Sigma Aldrich) as the silver ion source. Formic acid (HCOOH, 98% Fluka) and sodium formate (HCOONa, 99.3%, Fisher) were used as formate sources. Silver nanopowder (576,832, >99.5%, Sigma Aldrich) was used as received. Ultrapure deionized water was used for all experiments and prepared using a Nanopure® (18.3 MΩ-cm) treatment system.

2.2. P90/Ag synthesis

P90 was loaded with silver by an ultraviolet (UV) photoreduction method that reduces silver ions on the surface of P90. Briefly, 5 g of P90 was added to 500 mL of water and then bath sonicated (80 W/L, 40 kHz) for 30 min. An 8-mL aliquot of methanol (CH_3OH, 99.9%, Fisher) was added to the suspension to act as a hole scavenger to increase the rate of silver deposition. The pH was adjusted to 10–11 using sodium hydroxide (NaOH, 97.0%, EMD) to form negative surface charges on P90 to assist with silver cation adsorption. The appropriate mass of silver ions for 0.5–5% loading from silver nitrate was then added to the suspension and mixed in the dark for 30 min to allow for adsorption. After mixing, the suspension was purged with argon for 15 min to remove dissolved oxygen (DO). The suspension was then covered, transferred to a photoreactor containing a 450-W medium pressure mercury lamp (Hanovia, PC451.050), and irradiated for approximately 30 min. After sufficient washing, the sample was dried in an air oven at 90 °C for 24 h and then ground, giving a light purple powder.

2.3. Photocatalyst characterization

Images were obtained using a high-resolution scanning transmission electron microscope (STEM or TEM) with energy dispersive X-ray capabilities (EDS) (STEM Phillips CM-200). Surface elemental composition and chemical state were analyzed using X-ray photoelectron spectroscopy (XPS) performed on a ESCALAB 220i-XL (Vacuum Generators, USA) with a monochromatic Al K_α source at $h\nu$ = 1486 eV and a base pressure = 7×10^{-10} mbar. Ultraviolet–visible light diffuse reflectance (UV–vis DR) spectrums were obtained on a Lambda 18 (Perkin Elmer, USA) with a 150 mm integrating sphere accessory. The zeta potential was determined using the Phase Analysis Light Scattering Technique (ZetaPALS, Brookhaven, NY) in 10 mM KNO_3 background electrolyte. The specific surface area was obtained with the Branauer, Emmett and Teller (BET) model using a Tristar II 3020 automated gas adsorption analyzer (Micromeritics, USA). Inductively coupled plasma–mass spectrometry (ICP–MS) (Thermo X-Series 2, Thermo Fisher Scientific Inc., Waltham, MA) was used to determine the mass of Ag loaded onto the photocatalyst. Duplicate samples were digested in a microwave using concentrated nitric acid, diluted, and then injected into the ICP–MS.

2.4. Photocatalytic experiments

Photocatalytic experiments were performed using a 200-mL photoreactor with a UV lamp located in the center. A borosilicate sleeve was placed around the lamp to filter out light wavelengths less than 280 nm to avoid direct photolysis of nitrate or formate. This was done to elucidate photocatalytic mechanisms; removing the sleeve simply increased the rate of removal, and no change in by-products was observed. The UV light source was a 450-W (Ace Glass power supply, 7830-60) medium-pressure mercury–vapor lamp (Ace Glass, 7825-34; Hanovia PC451.050) that was placed in a double-walled quartz immersion well (Ace Glass, 7854-25). The system temperature was maintained at 25 °C using a chiller. For each run, the photocatalyst was suspended using magnetic stirring in a solution of ultrapure water containing nitrate and formate.

The experimental design matrix included a baseline experiment (pH = 2.5, initial nitrate concentration = 7.14 mM, initial formic acid concentration = 40 mM, P90/Ag(1%) dosage = 1 g/L), which was assumed to be optimal on the basis of previous studies [31]. From the baseline conditions, variables altered included photocatalyst concentration, silver loading, initial pH, initial nitrate concentration, and initial formic acid concentration; each was varied while keeping the other baseline conditions constant. P90/Ag(1%) dosage (0.1–1 g/L) and silver loading (0.5–5%) were varied to demonstrate their effect on the rate of nitrate removal and by-product selectivity. As a control, P90 (1 g/L) was mixed with 1% mass of Ag^0 nanoparticles to prove if a synergistic effect was present. The effect of pH was investigated at pH 2.5–10. pH was adjusted using the appropriate concentration of formic acid and sodium formate. The pH in control experiments containing no formate was adjusted using nitric acid (HNO_3). The effect of different nitrate and formate concentrations was investigated using three sets of experiments:

(1) the initial concentration of formic acid was varied from 20 to 80 mM while keeping the initial nitrate concentration (7.14 mM) constant; (2) the initial nitrate concentration was varied from 0.714 to 35.7 mM while keeping the initial formic acid to nitrate molar ratio (FNR), 5.6, constant (i.e., the initial formic acid concentration was 4–200 mM); and (3) the initial nitrate concentration was varied from 0.714 to 35.7 mM while keeping the initial concentration of formic acid (40 mm) constant. The experimental design matrix is shown in Table SI-1. Prior to irradiation, the sample was stirred in the dark for 1 h to eliminate non-photocatalytic removal (i.e., adsorption). On average, nitrate adsorption was <5% or ~2 mol/nm^2. During kinetic photocatalysis experiments, samples were collected over time, filtered using a 0.45-μm nylon membrane to remove the photocatalyst, and stored in amber glass vials in the dark at ~3 °C until analysis within 48 h.

2.5. Analytical methods

Samples were analyzed for nitrate (NO_3^-), nitrite (NO_2^-), ammonia (NH_4^+), and total dissolved nitrogen (TDN) to assess formation of aqueous by-products, and dissolved organic carbon (DOC) was measured to monitor changes in the concentration of formate (i.e., hole scavenger) over time. Ion chromatography was used to measure nitrate and nitrite anions (Dionex DX-120; AS12A column) and ammonium cations (Dionex IC-20; CS12A column) following EPA Standard Method 4110. TDN and DOC were measured using a total organic carbon/total nitrogen analyzer (Shimadzu TOC-V/ASI-V/TNM-1). Ion chromatography (Dionex DX-120; AS12A column) was used to confirm that all DOC present was formate and not an intermediate carbon compound. DO was measured using a handheld DO meter (YSI 550A). Previous studies on the photocatalytic reduction of nitrate detected only nitrite, ammonium, dinitrogen (N_2), and nitrous oxide (N_2O) as by-products [23,27,30,31,34,35,40,41]; therefore, the mass of gaseous nitrogen by-products was approximated on the basis of a nitrogen mass balance using nitrate, nitrite, ammonia, and TDN. Because this study focused on finished water quality (i.e., aqueous species for drinking water), the ratio of greenhouse gas (N_2O) to inert gas (N_2) was not measured. The selectivity toward nitrite (1), ammonium (2), and N gaseous by-products (3) were defined according to:

$$S(NO_2^-) = \frac{[NO_2^-]}{[NO_3^-]_0 - [NO_3^-]_t}, \quad (1)$$

$$S(NH_4^+) = \frac{[NH_4^+]}{[NO_3^-]_0 - [NO_3^-]_t}, \quad (2)$$

and

$$S(N_{gas}) = \frac{[NO_3^-]_0 - [NO_3^-]_t - [NO_2^-]_t - [NH_4^-]_t}{[NO_3^-]_0 - [NO_3^-]_t} \quad (3)$$

where $[X]_0$ is the concentration at time = 0 and $[X]_t$ is the concentration at time = t.

2.6. Lamp irradiance measurements

The lamp irradiance was measured using a UV–vis fiber optic spectrometer (Avantes AvaSpec-2048) adapted with a cosine corrector. Irradiance was measured at a distance halfway between the lamp and reactor wall (1 cm) and at multiple points from the bottom to the top of the reactor to obtain the average irradiance. For this study, the total lamp irradiance in ultrapure water from 280 to 1050 nm was 29.2 mW/cm^2. With a bandgap of ~3.2 eV [39], the total irradiance absorbable by P90 (280–388 nm) was 6.5 mW/cm^2, or approximately 22% of the total lamp irradiance. Only the wavelengths absorbed by P90 were used for reporting experimental results. To make the results comparable with other materials and similar studies, they are reported as a function of irradiation rather than time. Because a polychromatic lamp was used, the irradiation is reported not as an energy fluence (e.g., J/cm^2) but as a photon fluence (P90 absorbable) to account for differences in photon energies.

3. Results and discussion

3.1. Photocatalyst characterization

Samples were characterized using microscopy, elemental, and surface analyses. Fig. 1 shows TEM images of P90 with and without silver loading. Pristine P90 consists of nanocrystallites approximately 10–30 nm in diameter and has a distinct tetragonal structure (Fig. 1a). After loading with silver there was an obvious change in the morphology of the crystallites owing to surface coverage with silver islands, which was confirmed by EDS (Fig. 1b). The silver nanoparticles were approximately 2–3 nm in diameter.

XPS was used to characterize the chemical state and composition of the silver nanoparticles. XPS data was collected through the 3d core excitation for silver (Fig. SI-1). The binding energy of bulk silver is 368 eV [42]. The $3d_{5/2}$ peak is slightly asymmetric, indicating that oxygen may be associated with the silver. Peak fitting showed that a dual curve fit was appropriate for the 3d spectrum. The true positions of Ag^0 and Ag_xO_y are difficult to determine though because the particle size varies. A silver oxide shell is likely given the poor stability of silver in air. The silver oxide content obtained from XPS spectra could be low because of the small thickness of the shell. The inelastic mean free path for silver is approximately 5.7 nm at 1486 eV [43], which is greater than the average silver particle size of 3 nm. Although XPS is a surface characterization analysis, the particle is small enough that it may be considered as a bulk characterization in this case. The results suggest that the silver nanoparticles have a metallic core (Ag^0) with an oxide shell, most likely Ag_2O. This oxide shell may have unknown effects such as a change in the tunneling rate of the electrons, stability of the silver under aqueous conditions, and surface interaction with nitrate, its reduced intermediates and other ions in solution.

UV–vis absorbance was represented using the Kubelka–Munk function for the diffuse reflectance spectrum (Fig. SI-2; Eq. (4))

$$f(R) = \frac{(1 - R_\infty)^2}{2R_\infty} = \frac{k}{s} \quad (4)$$

where R_∞ is the absolute reflectance, k is the molar absorption coefficient, and s is the scattering coefficient. P90 absorbed wavelengths less than 400 nm. The addition of silver nanoparticles resulted in an additional absorption peak around 500 nm, which was attributed to a localized surface plasmon resonance (LSPR). The LSPR of silver nanoparticles is generally around 400 nm [44], but is red-shifted with increasing Ag_2O shell thickness [45,46], which would explain the peak position at 500 nm and also provides further evidence for the presence of an oxide shell. Normally, the LSPR would account for additional photon absorption and consequently, an increase in the quantum yield [47]. However, the presence of an oxide shell may reduce the LSPR effects significantly [48]. Also, for photocatalysts loaded with metal nanoparticles under redox conditions, the LSPR effects can be dominated by charging due to electron trapping [49]. Therefore, we did not account for any additional absorption caused by LSPR when calculating the rates as a function of photon absorption.

Zeta potential (ξ) analysis was performed from pH 2.5–10.5 (Fig. SI-3). P90/Ag(1%) had a point of zero charge (pH_{zpc}) of 7.1, compared with 6.4 for P90 [39]. Adding silver also resulted in a higher absolute surface charge under both acidic and basic conditions. For example, at pH = 4, P90/Ag(1%) was ~47 mV, and P90 was

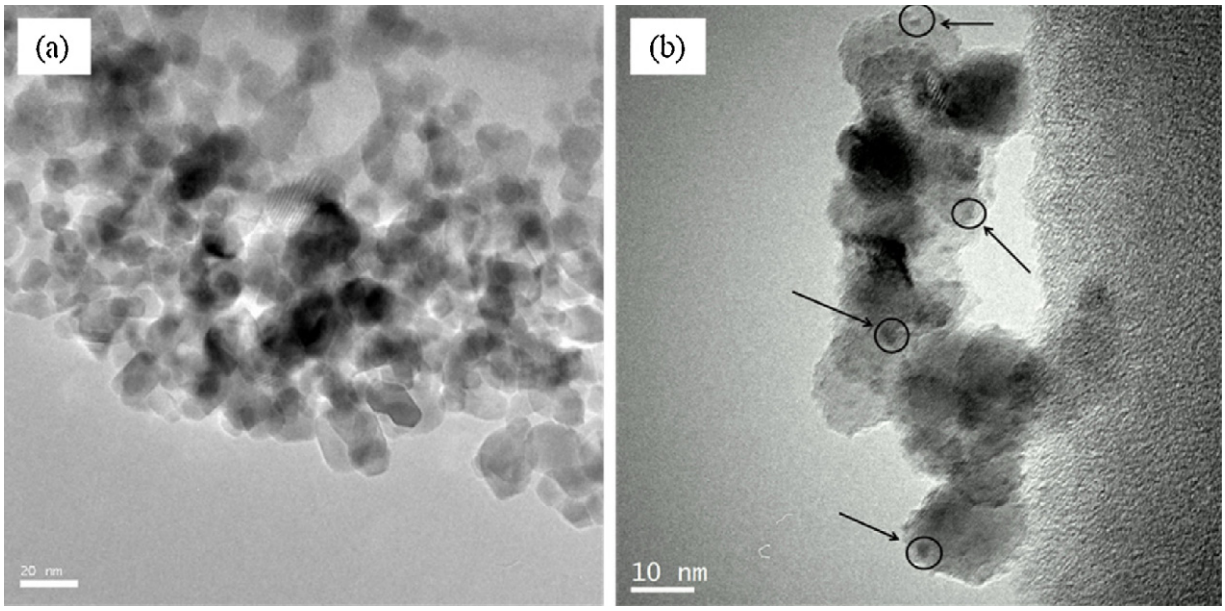

Fig. 1. TEM images of (a) P90 and (b) P90/Ag(5%). Black particles in (b) are silver nanoparticles; some are highlighted with circles (~2–3 nm).

~31 mV (Fig. SI-3). A higher pH_{zpc} results in a lower adsorption energy requirement for anions when the pH is below the pH_{zpc}.

BET results showed that the specific surface areas for 0, 0.5, 1, 2, and 5% silver loadings were 104, 101, 94, 77, and 73 m^2/g, respectively. These results indicate that as the percentage of silver is increased, the surface area decreases. Because P90 is non-porous, this suggests that silver particles fill either surface sites on P90 that would otherwise be attributed to higher surface area or voids between P90 aggregates.

ICP–MS results of acid-digested photocatalysts revealed silver mass loadings of 0.52, 1.10, 2.16, and 5.27% for theoretical loadings of 0.5, 1, 2, and 5%, respectively, indicating that more than 100% of Ag^+ was photodeposited onto the P90 surface, which was attributed to experimental error.

3.2. Photocatalytic removal of nitrate and formate

When formic acid and nitrate were mixed under dark or irradiated conditions ($\lambda > 280$ nm), no nitrate reduction occurred without a photocatalyst. Therefore, formic acid does not act as a direct reductant under these experimental conditions; rather, it acts as a hole scavenger. Fig. 2 shows the concentrations of nitrogen compounds and formate as a function of photon fluence for the baseline experiment. Nitrite forms as an intermediate, and ammonium is a by-product; ammonium does not appear until after some nitrite has formed, which indicates that nitrate reduction is a step-wise process. After complete nitrate removal, the sum of NO_3^-, NO_2^-, and NH_4^+ accounted for ~90% of TDN for aqueous N species. The difference may be attributed to some nitrous acid (HNO_2, $pK_a = 3.3$) volatilization when samples were acidified for TDN measurement. This means that accumulation of significant amounts of other aqueous inorganic (e.g., hydroxylamine) or organic nitrogen species as aqueous intermediates or by-products from reactions with the hole scavenger are unlikely, which is in good agreement with previous studies [31,34]. Time-dependent concentrations of both nitrate and formate fit well ($R^2 > 0.95$) to a pseudo-first-order rate (Fig. SI-4).

3.3. Effect of photocatalyst dosage and silver loading

When the suspended concentration of P90/Ag(1%) is increased, the rate of nitrate disappearance increases, reaching an apparent maximum at approximately 1 g/L (18.8 m^2), at which point the rate begins to decrease gradually (Fig. SI-5a). The resulting inverse U-shaped curve indicates that increasing the photocatalyst surface area in the reactor results in improved nitrate reduction, but only to a limiting concentration at which the rate decreased, presumably due to irradiation shielding.

Loading silver onto P90 improved the rate of nitrate removal significantly (Fig. SI-5b). For example, loading 1% silver onto P90 increased the pseudo-first-order rate constant for nitrate, $k_{nitrate}$, fivefold from 0.031 to 0.16 $cm^2/10^{18}$ photons $[T]^{-1}$. Above approximately 2% loading, $k_{nitrate}$ began to decrease. This may be attributed to too much P90 coverage, which would decrease the available irradiation area and cover up TiO_2 surface sites necessary for chemical reactions. Too much silver may also cause an increase in the silver particle size owing to silver cluster growth, which decreases its ability to store electrons [38]. The silver nanoparticles appeared to be adhered to the P90 surface (Fig. 1b), but the observed rate increase may have been caused by a synergistic effect between Ag^0 particles and P90 and not a semiconductor-metal contact. However, when Ag^0 nanoparticles were mixed with P90 there was no improvement of the nitrate reduction rate, suggesting that indeed

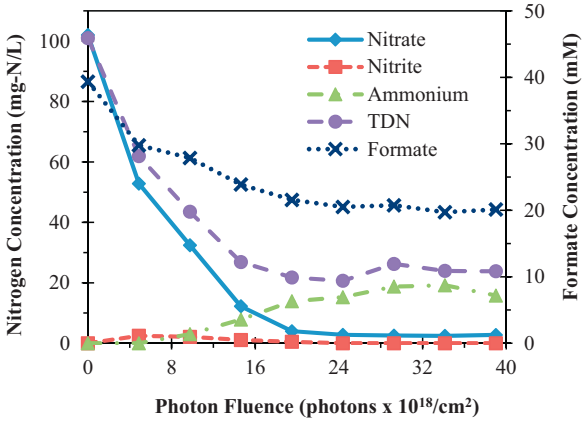

Fig. 2. Concentrations of nitrogen compounds and formate as functions of photon fluence for the baseline experiment (7.14 mM NO_3^-, 40 mM HCOOH, 1 g/L P90/Ag(1%), pH = 2.5).

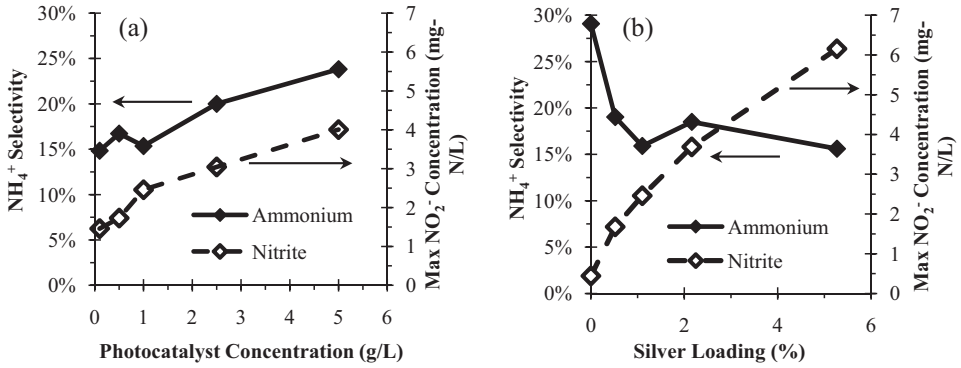

Fig. 3. NH4+ selectivity and the maximum NO_2^- concentration as a function of (a) photocatalyst concentration (P90/Ag) in the reactor and (b) the percent mass of silver loaded onto P90. The silver loading in (a) is kept constant at 1%, and the photocatalyst concentration in (b) is constant at 1 g/L. Initial concentrations for nitrate (100 mg-N/L) and formic acid (40 mM, pH = 2.5) were constant. Photon fluence = 29 × 1018 photons/cm^2.

the improvement was due to a direct semiconductor-metal contact.

Fig. 3 shows the ammonium selectivity and the maximum nitrite concentration as functions of (a) photocatalyst concentration (P90/Ag(1%)) and (b) the percent mass of silver loaded onto P90. Because nitrite was an intermediate species, the selectivity for each sample was zero after complete nitrate removal. Therefore, to compare the differences in nitrite intermediate formation in each sample, the maximum measured nitrite concentration was reported instead of selectivity. When the concentration of P90/Ag(1%) increased, both ammonium selectivity and the maximum nitrite concentration increased (Fig. 3a). When the photocatalyst concentration was held constant and the percent silver loading increased, the selectivity to ammonium decreased, and the maximum nitrite concentration increased (Fig. 3b). Adding a small amount of silver (0.5%) to P90 decreased the ammonium selectivity significantly (i.e., 29–19%), but it also increased the maximum nitrite intermediate concentration from 0.5 to 1.7 mg-N/L. Further increase in the mass percentage of silver did not significantly change the NH_4^+ selectivity, but the maximum nitrite concentration continued to increase. The improved reaction rate may be explained by silver's ability to build up excess electrons [39], thus promoting the reduction process. However, the rate of nitrite reduction to other nitrogen species decreased, suggesting that P90 sites, which decreased in number as silver loading increased, are responsible for nitrite reduction to further nitrogen intermediates.

3.4. Effect of system pH on rate and selectivity

Across acidic to neutral pH conditions (2.5–6.8), approximately 100% nitrate removal was observed after 29 × 10^{18} photons/cm^2. Under alkaline conditions (pH = 10), no nitrate or formate removal was observed. $k_{nitrate}$ and the pseudo-first-order rate constant for formate, $k_{formate}$, decreased with increasing pH (Table SI-1). For example, at pH = 2.5, $k_{nitrate}$ and $k_{formate}$ were 0.16 and 0.026 cm^2/10^{18} photons, respectively, and when the pH was increased to 6.8, $k_{nitrate}$ and $k_{formate}$ decreased to 0.068 and 0.0083 cm^2/10^{18} photons, respectively. Two processes could cause this decrease in observed pseudo-first-order removal rate, as increasing pH (1) decreases the number of protons available for reduction reactions and (2) increases the net negative surface charge of P90.

The multi-electron reduction of nitrate is more thermodynamically favorable (Eqs. (5)–(7)) than the single-electron reduction of nitrate (Eq. (8), E^0 = –1.1 V [50]). However, the multi-electron reaction requires protons, thus making pH a factor. At acidic pH, the reduction rate was faster than at neutral pH, and at alkaline pH, where the proton concentration was low, no nitrate removal was observed. Furthermore, P90 alone did not reduce nitrate at ambient pH [39], but the addition of silver made nitrate reduction possible. This suggests that silver may localize protons at its surface and reduce the overpotential for nitrate reduction.

If nitrate and formate require direct electron and hole transfers, respectively, then their adsorption to the photocatalyst must occur before charge transfer. When the pH was 2.5, 6.8, and 10, the zeta potential of P90/Ag(1%) was +44, +6, and −46 mV, respectively. At pH = 2.5, the surface charge is highly positive, which promotes the adsorption of nitrate and formate by decreasing the energetic requirement for anion adsorption. At pH = 6.8 and in the absence of silver (i.e., P90 alone), the zeta potential was negative (ξ = −4 mV), and nitrate removal was not observed. With 1% silver on the P90 surface, the zeta potential was shifted to positive (ξ = +6 mV), anion adsorption thermodynamic requirements were still favorable, and nitrate removal was observed. At pH = 10, the thermodynamic adsorption barrier for anions was much greater, and nitrate removal was not observed. These results suggest that adsorption of both formate and nitrate is important for direct transfer of charge carriers from the photocatalyst to the ion.

Fig. 4 shows the selectivity for nitrite and ammonium at different pH levels after 39 × 10^{18} photons/cm^2. Each data point represents the final sample with approximately 100% nitrate removal. When pH ≤ 3.5, nitrite was an intermediate, presumably in the protonated form (Eq. (9)), and ammonium was the main aqueous by-product (Eq. (6)). Nitrogen gases, which were assumed to be N_2 (Eq. (7)) and N_2O (Eq. (10)), were presumably the main overall by-product. At 3.5 < pH < 5, nitrite became the dominant by-product in addition to some ammonium and nitrogen gases. At pH > 5, nitrite was the only by-product observed. One possible

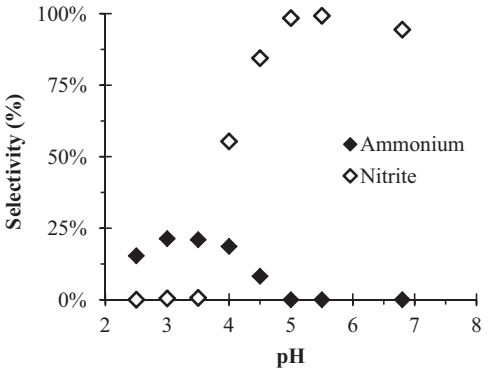

Fig. 4. Nitrite and ammonium selectivity at different initial pH after 39 × 1018 photons/cm^2 (56 min) of irradiation and ~100% nitrate removal. Initial concentrations were 100 mg-N/L nitrate, 40 mM formate, and 1 g/L P90/Ag (1%).

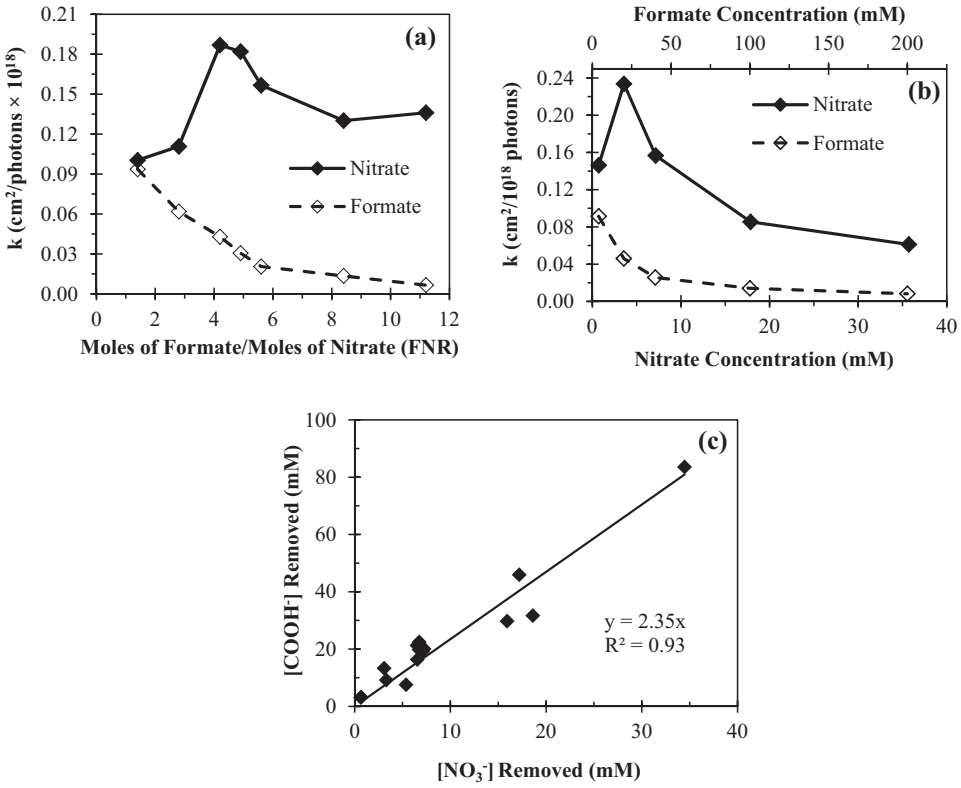

Fig. 5. The pseudo-first-order rate constant, k, at pH = 2.5–2.7 for nitrate and formate as a function of (a) FNR at a constant initial nitrate concentration, 7.14 mM, and (b) nitrate and formate concentration at a constant FNR, 5.6. (c) Relationship between moles of formate removed and moles of nitrate removed for all of these experiments performed at pH = 2.5.

explanation for the sudden by-product switch between pH ~3.5 and 4 is that the pK_a for HNO_2/NO_2^- is approximately 3.3, and HNO_2 is known to disproportionate to NO and NO_2 at a fast rate (Eq. (11), $k = 13.4 \times 10^8\ M^{-1}\ s^{-1}$) [51]; this may be the key limiting step for further reduction to N_2, N_2O, and NH_4^+. Therefore, a pH of ~3.5 can be used instead of pH = 2.5 to reduce formation of more harmful by-products (e.g., NH_4^+) while maintaining a similar rate of nitrate removal.

$$NO_3^- + 2e^- + 2H^+ \rightarrow NO_2^- + H_2O \quad (E^0 = 0.84\,V) \tag{5}$$

$$NO_3^- + 8e^- + 10^+ \rightarrow NH_4^+ + 3H_2O \quad (E^0 = 0.88\,V) \tag{6}$$

$$2NO^- + 10e^- + 12H^+ \rightarrow N_2 + 6H_2O \quad (E^0 = 1.25\,V) \tag{7}$$

$$NO_3^- + e^- \rightarrow NO_3^{2-} \quad (E^0 = -1.1\,V) \tag{8}$$

$$NO_3^- + 2e^- \rightarrow NO_3^{2-} \quad (E^0 = 0.94\,V, pK_a = 3.3) \tag{9}$$

$$2NO_3^- + 8e^- + 10H^+ \rightarrow N_2O + 5H_2O \quad (E^0 = 1.12\,V) \tag{10}$$

$$2HNO_2 \rightleftharpoons NO + NO_2 + H_2O \tag{11}$$

3.5. Effect of varying nitrate and formic acid concentrations

Fig. 5a shows $k_{nitrate}$ and $k_{formate}$ as functions of the initial formic acid to nitrate molar ratio (FNR) at a constant initial nitrate concentration of 7.14 mM. Complete nitrate removal was achieved at each FNR. For $k_{nitrate}$, increasing the FNR yielded no significant improvement; a minimum of 0.10 $cm^2/10^{18}$ photons occurred at FNR = 1.4, and a maximum of 0.19 $cm^2/10^{18}$ photons occurred at FNR = 4.2. However, when the FNR was less than 2.8, nitrate removal ceased after formate was removed from the system, indicating that the FNR was less than the stoichiometric requirement. $k_{formate}$ decreased with increasing FNR, indicating that increasing the formate concentration decreases the ability of the system to remove formate.

Fig. 5b shows $k_{nitrate}$ and $k_{formate}$ as functions of the initial formate and nitrate concentrations at a constant FNR of 5.6. Except at low nitrate concentrations (<10 mg-N/L), increasing the initial concentrations of nitrate and formate decreased both of their removal rates. We suspect this decrease was a result of an increase in ionic strength, which would decrease the ability of the photocatalyst to adsorb nitrate and formate ions. These results are important for modeling the reaction and transitioning experiments to larger scale experiments.

3.6. Controlling hole scavenger removal

For drinking water applications, residual organic hole scavenger (e.g., formate) is undesirable. Consequently, removal of the hole scavenger from the system is necessary, but doing so requires knowing the stoichiometric FNR. Fig. 5c shows the relationship between moles of formic acid removed and moles of nitrate removed for all experiments at pH = 2.5. A simple linear regression model was used to fit the data ($R^2 = 0.93$); the slope indicates the average stoichiometric ratio (Fig. 5c). This suggests that the average experimental FNR for all samples is approximately 2.4, which is close to the theoretical value of 2.7 for 85% N_2 and 15% NH_4^+ selectivity. This is also in good agreement with the formate requirement for biological denitrification [52].

By knowing the required stoichiometric FNR, we can adjust the photocatalyst concentration and the formic acid concentration such that 1:1 nitrate/formate removal and optimal kinetics are achieved. For example, for 17.85 mM nitrate (250 mg-N/L), 1 g/L P90/Ag, and FNR = 2.5, the required formic acid concentration would be 44.6 mM. When this was tested at pH = 2.5, similar $k_{nitrate}$ (0.040 $cm^2/10^{18}$ photons) and $k_{formate}$ (0.043 $cm^2/10^{18}$ photons) rates were obtained. Nitrate and formate were removed at a 0.94:1 ratio, which shows that both nitrate and the hole scavenger can be

removed from the system by controlling the experimental parameters. Also, less than the required FNR can be added and partial nitrate removal still achieved (i.e., Fig. 5a), which is important in a continuous flow system.

3.7. Proposed mechanisms of formic acid as a hole scavenger

Some studies have suggested that strong reducing radicals produced from photocatalytic oxidation of formate, such as the carbon dioxide radical, $CO_2^{\bullet-}$ [31,34] ($E^0 = -1.8$ V [53]), and the hydrogen radical, H• [35] ($E^0 = -2.3$ V [54]), are responsible for nitrate reduction, rather than e_{cb}^-. Electron paramagnetic resonance (EPR) analysis showed that photocatalytic oxidation of formate over TiO_2 produced only $CO_2^{\bullet-}$ and that no H• was present [55]. H•/H_2 reduction is more likely to occur over a hydrogenation co-catalyst such as Pd or Pt [35,56].

Nitrate reduction may proceed step-wise through either a one-electron reduction or a multi-electron reduction. If we examine the case in which nitrate is reduced to nitrite, two electrons are required in total (Eq. (5)). Consequently, to maintain electroneutrality and avoid recombination, two holes would have to be reduced by one formic acid molecule (Eqs. (12) and (13)). Formic acid first adsorbs on the surface of TiO_2 and disproportionates to the formate anion and a proton (Eq. (14), $pK_a = 3.74$) [57]. TiO_2 is photoexcited, forming an h_{vb}^+ and an e_{cb}^- (Eq. (15)). Formate reacts with one h_{vb}^+ to form the carbon dioxide anion radical, $CO_2^{\bullet-}$ (Eq. (16)) [53,55,58–60], which is protonated below pH = 1.4 [61]. If $CO_2^{\bullet-}$ alone was responsible for nitrate reduction to nitrite, then 1 mol of nitrate would require 2 mol of formate (i.e., $2HCOO^- = 2CO_2^{\bullet-} = 2e^-$; FNR = 2). However, experimental evidence presented herein has shown that the FNR is actually ~1.4, which means that $CO_2^{\bullet-}$ is not solely responsible for the reduction of nitrate, and an additional electron is being used for this reduction reaction.

After $CO_2^{\bullet-}$ forms, we hypothesize that the further redox event may occur under three different scenarios: (1) $CO_2^{\bullet-}$ reacts with an h_{vb}^+ (Eq. (17)), and two e_{cb}^- reduce nitrate to nitrite; (2) $CO_2^{\bullet-}$ injects an electron into the conduction band of TiO_2 (Eq. (18)), and two e_{cb}^- reduce nitrate to nitrite; or (3) $CO_2^{\bullet-}$ reacts directly with nitrate to form NO_3^{2-} (Eq. (19)), which is then further reduced to NO_2^- using one e_{cb}^-.

$$HCOOH + 2h_{vb}^+ \rightarrow CO_2 + 2H^+ + 2e^- \quad (E^0 = -0.199\,V) \tag{12}$$

$$NO^- + HCOOH \rightarrow NO_2^- + CO_2 + H_2O \tag{13}$$

$$HCOOH_{ads} \rightarrow H_{ads}^+ + COOH_{ads}^- \tag{14}$$

$$TiO_2 + h\nu \rightarrow h_{vb}^+ + e_{cb}^- \tag{15}$$

$$HCOO_{ads}^- + h_{vb}^+ \rightarrow HCO_2^{\bullet} \rightleftharpoons H^+ + CO_2^{\bullet-} \quad (pK_a = 1.4) \tag{16}$$

$$CO_2^{\bullet-} + h_{vb}^+ \rightarrow CO_2 \tag{17}$$

$$CO_2^{\bullet-} + h_{vb}^+ \rightarrow CO_2 \quad (\text{injectiontoconductionband}) \tag{18}$$

$$CO_2^{\bullet-} + NO_3^- \rightarrow CO_2 + NO_3^{2-} \tag{19}$$

$$CO_2^{\bullet-} + O_2 \rightarrow CO_2 + O_2^{\bullet-} \tag{20}$$

If nitrate reduction occurs via a multi-electron transfer, then Eqs. (17) and (18) are most probable. If nitrate reduction occurs via a step-wise one-electron reduction to NO_3^{2-}, which has a high reduction potential ($E^0 = -1.1$ V), then Eq. (19) is the probable pathway because of the low potential of e_{cb}^- ($E^0 = -0.25$ V, Fig. SI-6). Results presented herein indicate that addition of a silver co-catalyst enhances nitrate reduction, presumably through electron storage, which would agree with Eqs. (17) and (18). Furthermore, previous studies have shown that photocatalytic oxidation of formate can have a current doubling effect (Eq. (18)) [58,62,63]. However, an electron scavenger such as nitrate or oxygen can quench the radical before this occurs (i.e., Eq. (20)). Reaction with oxygen is unlikely to be the dominant process, however, because nitrate is a more effective electron scavenger than oxygen [64], and nitrate removal was still observed with oxygen present in our system. Without doing further in-depth analytical studies, determining which scenario is occurring is difficult, but given the currently available information, nitrate reduction seems to proceed through a multi-electron reduction using e_{cb}^- and not radicals.

3.8. Implications for drinking water treatment

The results presented herein are integral to advancing photocatalytic nitrate treatment for drinking water systems. For TiO_2, the addition of an organic electron donor is necessary, which poses a problem for drinking water treatment. However, we have shown experimentally the required stoichiometric ratio of formate such that effluent DOC concentrations can be maintained during nitrate treatment. For TiO_2, pH still presents a barrier for drinking water treatment, and although the final pH is near 5, it would still need to be adjusted post-treatment, which can be costly.

To overcome some of the limitations of TiO_2 highlighted in this study and move toward direct drinking water treatment, ultimately, new materials must be developed. The results presented herein will be important for designing these new photocatalysts. First, we have given evidence that radicals are unlikely to be responsible for nitrate reduction, so a photocatalyst base material with the proper Fermi level must be selected to meet the thermodynamic requirements. Second, pH was a factor in our experiments, so proton localization at the reaction sites will be important for treatment at ambient pH and for achieving innocuous by-products, which can be accomplished by selecting the proper co-catalysts (e.g., Ag, Cu). Although photocatalysis is not fully suitable for drinking water applications yet, P90/Ag removes nitrate efficiently and with a high selectivity, and it would be appropriate for offline treatment, such as that of ion-exchange brines.

Acknowledgements

This research was supported by the National Science Foundation (CBET 1132779). Graduate student support was partially provided by a Science Foundation Arizona fellowship. Materials were characterized in the LeRoy Eyring Center for Solid State Science at Arizona State University.

Appendix A. Supplementary data

Supplementary data associated with this article can be found, in the online version, at http://dx.doi.org/10.1016/j.apcatb.2013.01.042.

References

[1] L.J. Guillette, T.M. Edwards, Integrative and Comparative Biology 45 (2005) 19–27.
[2] H.J. Hamlin, B.C. Moore, T.M. Edwards, I.L.V. Larkin, A. Boggs, W.J. High, K.L. Main, L.J. Guillette, Aquaculture 281 (2008) 118–125.
[3] H.J. Hamlin, Aquaculture 253 (2006) 688–693.
[4] K.R. Burow, B.T. Nolan, M.G. Rupert, N.M. Dubrovsky, Environmental Science & Technology 44 (2010) 4988–4997.
[5] B. Nolan, Epidemiology 15 (2004), S109-S109.
[6] B.T. Nolan, K.J. Hitt, Environmental Science & Technology 40 (2006) 7834–7840.
[7] B.T. Nolan, L.J. Puckett, L.W. Ma, C.T. Green, E.R. Bayless, R.W. Malone, Journal of Environmental Quality 39 (2010) 1051–1065.
[8] B.T. Nolan, J.D. Stoner, Environmental Science & Technology 34 (2000) 1156–1165.
[9] M.G. Rupert, Journal of Environmental Quality 37 (2008) S240–S248.

[10] C. Seidel, C., Gorman, J.L., Darby, V.B. Jensen, An Assessment of the State of Nitrate Treatment Alternatives: Final Report, American Water Works Association, 2011.
[11] M.R. Hoffmann, S.T. Martin, W.Y. Choi, D.W. Bahnemann, Chemical Reviews 95 (1995) 69–96.
[12] A. Kudo, K. Domen, K. Maruya, T. Onishi, Chemistry Letters 16 (6) (1987) 1019–1022.
[13] A. Kudo, K. Domen, K.-i. Maruya, T. Onishi, Journal of Catalysis 135 (1992) 300–303.
[14] K.T. Ranjit, R. Krishnamoorthy, B. Viswanathan, Journal of Photochemistry and Photobiology A: Chemistry 81 (1994) 55–58.
[15] K.T. Ranjit, T.K. Varadarajan, B. Viswanathan, Journal of Photochemistry and Photobiology A: Chemistry 89 (1995) 67–68.
[16] K.T. Ranjit, R. Krishnamoorthy, T.K. Varadarajan, B. Viswanathan, ournal of Photochemistry and Photobiology A: Chemistry 86 (1995) 185–189.
[17] K.T. Ranjit, T.K. Varadarajan, B. Viswanathan, Indian Journal of Chemistry Section A-Inorganic Bio-Inorganic Physical Theoretical & Analytical Chemistry 35 (1996) 177–181.
[18] T. Sato, K.I. Sato, Y. Fujishiro, T. Yoshioka, A. Okuwaki, Journal of Chemical Technology and Biotechnology 67 (1996) 345–349.
[19] K.T. Ranjit, B. Viswanathan, Journal of Photochemistry and Photobiology A: Chemistry 108 (1997) 73–78.
[20] K.T. Ranjit, B. Viswanathan, Journal of Photochemistry and Photobiology A: Chemistry 107 (1997) 215–220.
[21] Y. Li, F. Wasgestian, Journal of Photochemistry and Photobiology A: Chemistry 112 (1998) 255–259.
[22] B. Bems, F.C. Jentoft, R. Schlogl, Applied Catalysis B: Environmental 20 (1999) 155–163.
[23] H. Kominami, A. Furusho, S. Murakami, H. Inoue, Y. Kera, B. Ohtani, Catalysis Letters 76 (2001) 31–34.
[24] M. Penpolcharoen, R. Amal, M. Brungs, Journal of Nanoparticle Research 3 (2001) 289–302.
[25] S. Tawkaew, S. Yin, T. Sato, International Journal of Inorganic Materials 3 (2001) 855–859.
[26] O. Hamanoi, A. Kudo, Chemistry Letters 31 (8) (2002) 838–839.
[27] H. Kato, A. Kudo, Physical Chemistry Chemical Physics 4 (2002) 2833–2838.
[28] W.L. Gao, R.C. Jin, M.X. Chen, X.X. Guan, H.S. Zeng, F.X. Zhang, N.J. Guan, Catalysis Today 90 (2004) 331–336.
[29] R.C. Jin, W.L. Gao, J.X. Chen, H.S. Zeng, F.X. Zhang, Z.G. Liu, N.J. Guan, Journal of Photochemistry and Photobiology A: Chemistry 162 (2004) 585–590.
[30] H. Kominami, T. Nakaseko, Y. Shimada, A. Furusho, H. Inoue, S. Murakami, Y. Kera, B. Ohtani, Chemical Communications 41 (23) (2005) 2933–2935.
[31] F.X. Zhang, R.C. Jin, J.X. Chen, C.Z. Shao, W.L. Gao, L.D. Li, N.J. Guan, Journal of Catalysis 232 (2005) 424–431.
[32] S. Rengaraj, X.Z. Li, Chemosphere 66 (2007) 930–938.
[33] L.F. Liu, X.Y. Dong, F.L. Yang, J.C. Yu, Chinese Journal of Inorganic Chemistry 24 (2008) 211–217.
[34] J. Sá, C.A. Agüera, S. Gross, J.A. Anderson, Applied Catalysis B: Environmental 85 (2009) 192–200.
[35] N. Wehbe, M. Jaafar, C. Guillard, J.M. Herrmann, S. Miachon, E. Puzenat, N. Guilhaume, Applied Catalysis A: General 368 (2009) 1–8.
[36] L.Y. Li, Z.Y. Xu, F.L. Liu, Y. Shao, J.H. Wang, H.Q. Wan, S.R. Zheng, Journal of Photochemistry and Photobiology A: Chemistry 212 (2010) 113–121.
[37] J.A. Anderson, Catalysis Today 175 (2011) 316–321.
[38] A. Takai, P.V. Kamat, ACS Nano 5 (2011) 7369–7376.
[39] K.D. Doudrick, O. Monzón, A. Mangonon, K. Hristovski, P.K. Westerhoff, ASCE Journal of Environmental Engineering 138 (2012) 852–861.
[40] H. Kominami, H. Gekko, K. Hashimoto, Physical Chemistry Chemical Physics 12 (2010) 15423–15427.
[41] W. Gao, R. Jin, J. Chen, X. Guan, H. Zeng, F. Zhang, N. Guan, Catalysis Today 90 (2004) 331–336.
[42] C.D. Wagner, A.V. Naumkin, A. Kraut-Vass, J.W. Allison, C.F J. Powell, J.R. Rumble, NIST X-ray Photoelectron Spectroscopy Database, Version 3.5, National Institute of Standards and Technology, Gaithersburg, MD, 2007.
[43] S. Tanuma, C.J. Powell, D.R. Penn, Surface and Interface Analysis 43 (2011) 689–713.
[44] U. Kreibig, Journal of Physics F: Metal Physics 4 (1974) 999–1014.
[45] K. Chatterjee, S. Banerjee, D. Chakravorty, Physical Review B 66 (2002), 085421.
[46] D.C. Schinca, L.B. Scaffardi, F.A. Videla, G.A. Torchia, P. Moreno, L. Roso, Journal of Physics D: Applied Physics 42 (2009), 215102.
[47] B.K. Vijayan, N.M. Dimitrijevic, J.S. Wu, K.A. Gray, Journal of Physical Chemistry C 114 (2010) 21262–21269.
[48] K. Awazu, M. Fujimaki, C. Rockstuhl, J. Tominaga, H. Murakami, Y. Ohki, N. Yoshida, T. Watanabe, Journal of the American Chemical Society 130 (2008) 1676–1680.
[49] H. Choi, W.T. Chen, P.V. Kamat, ACS Nano 6 (2012) 4418–4427.
[50] A.R. Cook, N. Dimitrijevic, B.W. Dreyfus, D. Meisel, L.A. Curtiss, D.M. Camaioni, Journal of Physical Chemistry A 105 (2001) 3658–3666.
[51] J.Y. Park, Y.N. Lee, Journal of Physical Chemistry 92 (1988) 6294–6302.
[52] R.L. Smith, D.N. Miller, M.H. Brooks, M.A. Widdowson, M.W. Killingstad, Environmental Science & Technology 35 (2001) 196–203.
[53] W.H. Koppenol, J.D. Rush, Journal of Physical Chemistry 91 (1987) 4429–4430.
[54] H.A. Schwarz, Journal of Chemical Education 58 (1981) 101–105.
[55] L.L. Perissinotti, M.A. Brusa, M.A. Grela, Langmuir 17 (2001) 8422–8427.
[56] U. Prüsse, M. Hähnlein, J. Daum, K.-D. Vorlop, Catalysis Today 55 (2000) 79–90.
[57] U. Diebold, Surface Science Reports 48 (2003) 53–229.
[58] T. Tachikawa, S. Tojo, M. Fujitsuka, T. Majima, Langmuir 20 (2004) 9441–9444.
[59] S. Somasundaram, Y. Ming, C.R. Chenthamarakshan, Z.A. Schelly, K. Rajeshwar, Journal of Physical Chemistry B 108 (2004) 4784–4788.
[60] J.R. Harbour, M.L. Hair, Journal of Physical Chemistry 83 (1979) 652–656.
[61] G.V. Buxton, R.M. Sellers, Journal of the Chemical Society-Faraday Transactions I 69 (1973) 555–559.
[62] N. Hykaway, W.M. Sears, H. Morisaki, S.R. Morrison, Journal of Physical Chemistry 90 (1986) 6663–6667.
[63] E.R. Carraway, A.J. Hoffman, M.R. Hoffmann, Environmental Science & Technology 28 (1994) 786–793.
[64] S.T. Martin, H. Herrmann, M.R. Hoffmann, Journal of the Chemical Society-Faraday Transactions 90 (1994) 3323–3330.